NOAA-20 VIIRS Relative Spectral Response Effects on Solar Diffuser Degradation and On-orbit Radiometric Calibration

Taeyoung Choi and Changyong Cao

***Abstract*—The Visible Infrared Imaging Radiometer Suite (VIIRS) on the National Oceanic and Atmospheric Administration-20 (NOAA-20) satellite performs on-orbit radiometric calibration based on regular Solar Diffuser (SD) observations illuminated by the Sun at the termination point near the South Pole. Due to exposure to the ultraviolet portion of the Solar irradiance spectrum, the SD Bidirectional Reflectance Distribution Function (BRDF) has been degrading over time. The SD degradation (called H-factor) was measured by the on-board calibrator called the Solar Diffuser Stability Monitor (SDSM). Nevertheless, over 2 years of operation, there have been systematic on-orbit calibration differences between the SD-based and independent moon-based calibration results.**

In this study, the NOAA VIIRS team used a Surface Roughness Rayleigh Scattering (SRRS) model as a baseline SD degradation, simulated on-orbit center wavelength-based approach of SD degradation and a new SDSM Relative Spectral Response (RSR) dependent SD degradation estimation method to evaluate the degradation. There were time-dependent growing differences between the SDSM RSR applied H-factors and center wavelength interpolated H-factors especially in the short wavelength detectors (SDSM detector 1 to 4). The NOAA-20 SD-based calibration coefficients (SD F-factors) were reprocessed using the RSR applied H-factors, and the new SD F-factors show similar long-term trends compared to the independent monthly lunar F-factors. The newly processed SD F-factor suggested that the NOAA-20 VIIRS detectors in the Reflective Solar Bands (M1-M11, and I1-I3) showed very stable responses within 0.5 percent level over the two years of on-orbit operation.

***Index Terms*—NOAA-20, VIIRS, Solar Diffuser (SD), Bidirectional Reflectance Distribution Function (BRDF) degradation, lunar calibration, Relative Spectral Response, RSR**

I. Introduction

THE Solar Diffuser (SD) calibration approach has been widely applied to polar orbiting Earth Observing sensors such as the historical Terra and Aqua Moderate Resolution Imaging Spectroradiometer (MODIS), Multiangle Imaging Spectro-Radiometer (MISR), Landsat Operational Land Imager (OLI), Suomi National Polar-orbiting Partnership (SNPP) VIIRS, and NOAA-20 VIIRS [1-7]. The SD became a standard on-orbit calibrator not only for Low Earth Orbit (LEO) sensors but also for geo-stationary (GEO) sensors such as the Advanced Himawari Imager (AHI) on Himawari 8 satellite and Advanced Baseline Imager (ABI) on GOES R satellites [8, 9].

The VIIRS sensor was intentionally designed to have the same Angle Of Incidence (AOI) of 60.4 degrees on the Half Angle Mirror (HAM) for both SD and Space View (SV) observations. Through the SV port, VIIRS can view the moon monthly except summer months from June to October. The primary purpose of having the same AOI for the SD and SV was to ensure lunar observations have the same viewing condition as SD observations to avoid different AOI problems with the Terra and Aqua MODIS sensors [2, 10, 11]. Even same HAM AOI for SD and SV observations, there were long-term trend differences between the lunar and SD radiometric calibrations [6, 12-16]. To resolve these radiometric calibration differences between the SD and moon, recent studies showed that the assumption of Lambertian surface for the SD was not applicable and there were angular dependencies of the SD reflectance degradation over time in the Solar Diffuser Stability Monitor (SDSM) SD view port and Rotating Telescope Assembly (RTA) view [17, 18]. On the other hand, the NOAA ocean color team assumed that there was a 'non-uniform SD degradation' in its Bidirectional Reflectance Distribution Function (BRDF) estimation and SDSM-based measurements provided biased degradation factors relative to the RTA view direction [17]. The mitigation strategy for the biases was called the 'hybrid method' and corrected the SD based calibration coefficient to the long-term lunar based calibration results by applying quadratic fits and ratios [19]. Another study by the National Aeronautics and Space Administration (NASA) VIIRS team suggested a numerical mitigation methodology called 'phenomenological model' for SNPP VIIRS using a higher order polynomials to remove annual oscillations in the H-factor estimations in terms of the partial derivatives of the solar elevation and azimuth angles [18]. It was named as 'phenomenological model' also corrected the long-term SD trends to the lunar calibration results by claiming that there were SD BRDF angular dependencies between the SDSM and RTA SD views.

Solar Diffuser material, commonly known as Spectralon ™ is assumed to provide highly diffused reflectance as a near-Lambertian surface in the visible (VIS), Near Infrared (NIR),

This paragraph of the first footnote will contain the date on which you submitted your paper for review. It will also contain support information, including sponsor and financial support acknowledgment. For example, "This work was supported in part by the U.S. Department of Commerce under Grant BS123456."

and Short-Wave InfraRed (SWIR) ranges [7]. Because of its near-ideal reflectance properties with the known degradation over time, the SD has provided a simple methodology to update on-orbit sensor radiometric calibration. As a known fact, the SD degrades faster especially due to exposure from the short wavelength UV side compared to the SWIR side [20, 21]. For accurate on-orbit radiometric calibration coefficients, the SD degradation needs to be measured correctly and compensated at selected wavelength locations determined over the SDSM detector wavelengths.

Previously, a physics-based model called Surface Roughness-induced Rayleigh Scattering (SRRS) was developed to explain surface physical properties that induced spectral degradation of the SNPP VIIRS SD [20]. In the SRRS model, the SD degradation was caused by surface roughness growth (inducing Rayleigh scattering) under the condition that the spectral wavelength is significantly larger than the roughness features on the surface. Consistent roughness rates were observed when it was applied to Terra/Aqua MODIS and SNPP VIIRS instruments and it proved validity of the SRRS model.

To simulate systematic long-term differences between SD and lunar calibrations, the NOAA VIIRS team developed a new SD degradation estimation algorithm from the Relative Spectral Response (RSR) function (H_{RSR}) and the SRRS model instead of using the conventional center wavelength interpolation. Often researchers use the term Spectral Band Adjustment Factor (or SBAF) to describe this type of correction, and it is widely used for other aspects of sensor radiometric calibration and cross-calibration[22, 23].

In Section II, on-orbit calibration algorithms are explained with equations. In section III, the center wavelength and RSR based SRRS model simulation steps are described. In results (section IV), the conventional SD degradation (H-factor) results are compared to RSR weighted H-factors (H_{RSR}). The H_{RSR} results showed significant time-dependent increases in the short wavelength SDSM detectors (detectors 1 to 3) up to 1.5 percent especially, with detector 1, around Days Since Launch (DSL) 800. After calculating the H_{RSR} function, it was applied to the radiometric calibration coefficients (SD F-factors) and compared to the lunar F-factors. The new SD F-factors became consistent to the corresponding lunar F-factors within 0.5 percent. New H_{RSR} algorithm provided very stable and consistent SD degradation estimations compared to the lunar calibration, which revealed superior stability of the NOAA-20 VIIRS Reflective Solar Band (RSB) detectors over the 2 years of operation.

II. VIIRS On-Orbit Radiometric Calibrations

A. SD Calibration

The VIIRS instrument has four On-board Calibrators (OBCs) as shown in Figure 1 for RSB and Thermal Emissive Bands (TEBs) calibration [24]. In the figure, the RTA rotates and views anticlockwise in sequence the blackbody (BB), SD, and SV. The RSB radiometric calibration is primarily dependent on the SD observations and the degradation of SD is monitored by

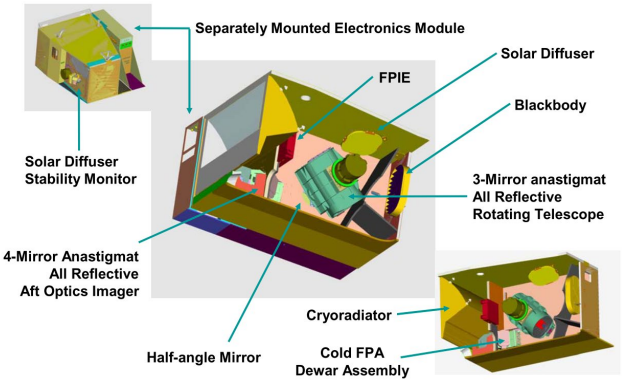

Figure 1. VIIRS Opto-Mechanical Module and OBC schematic [15].

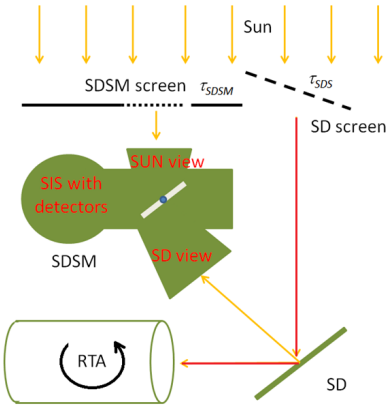

Figure 2. A simplified schematic of screens, SD, SDSM and RTA relations with illumination from the Sun [16].

SDSM. Figure 2 shows a simplified schematic of the SDSM. The SDSM tracks ratios between the Sun view Digital Count (DC) under an attenuation screen, called the SDSM Sun screen, and the DC of SD through the SD screen.

The normal SD degradation is calculated by Equation (1).

$$H\text{-}factor(t) = \frac{\mathrm{dc_{SD}}(t)\tau_{\mathrm{SDSM}}}{\mathrm{dc_{SUN}}(t)\mathrm{BRDF_{SDSM\_SD}}\tau_{\mathrm{SDS}}\cos(\theta_{\mathrm{inc}})\pi\sin^2\varphi} \quad (1)$$

In the denominator of Equation (1), $\mathrm{dc_{SUN}}$ is bias removed SDSM Sun view DC, τ_{SDS} is SD screen transmittance function, $\mathrm{BRDF_{SDSM\_SD}}$ is BRDF at the SDSM viewing angle to the SD surface, θ_{inc} is solar incident angle to the SD screen, and $\pi\sin^2\varphi$ is the solid angle of the SDSM SD view port. In the numerator, $\mathrm{dc_{SD}}$ is bias removed SD view DC, and τ_{SDSM} is SDSM Sun screen transmittance. Fundamentally, the H-factor is measured by the ratio of the SD responses that are normalized by the Sun as a reference with screen and BRDF angular corrections. After the VIIRS activation, unusual oscillations in the SD degradation (larger than 1% in all SDSM detectors) were detected and the problem was resolved by adding on-orbit regular SDSM data between the yaw-maneuver data to update the SDSM Sun view transmittance function [25-27].

The primary on-board radiometric calibration coefficients (F-factors) are calculated by the SD observations in Equation (2) through the RTA view that are indicated by red arrows in Figure 2.

$$F\text{-}factor(t) = \frac{\mathrm{RVS_{SD}}\cos(\theta_{\mathrm{inc}}(t))\left\{E_{\mathrm{sun}}\tau_{\mathrm{SDS}}\mathrm{BRDF_{RTA}}\frac{H(t)}{H(t_0)}\right\}}{C_0+C_1\mathrm{dn_{SD}}(t)+C_2\mathrm{dn_{SD}^2}(t)+C_3\mathrm{dn_{SD}^3}(t)} \quad (2)$$

In Equation (2), $\mathrm{RVS_{SD}}$ is Response Versus Scan (RVS) at SD viewing angle, E_{sun} is the solar irradiance value which is modulated by the VIIRS detector RSR, the $\tau_{\mathrm{SDS}}\mathrm{BRDF_{RTA}}$ is the SD screen modulated BRDF of the SD through the RTA view angle, $\frac{H(t)}{H(t_0)}$ is the normalized SD H-factor that linearly interpolated at the band-averaged VIIRS detector center wavelength from the SDSM detector center wavelengths, $C_{0,1,2,3}$ are DN to radiance conversion factors that are affected by the detector and electronics temperature from the prelaunch calibrations, and $\mathrm{dn_{SD}}(t)$ is the time-dependent SD observation. The H-factors at the VIIRS detector center wavelengths are linearly interpolated from the SDSM detector center wavelengths. The details of the center wavelength differences are explained in section III. Compared to 'dc' in Equation (1) for the SDSM, 'dn' is used for the VIIRS observations in Equation (2) to distinguish the viewing instruments.

B. *Lunar Calibration*

VIIRS can view the moon on a monthly basis through the SV port as shown in Figure 1. Usually, a spacecraft roll maneuver and sector rotation is required to place the moon at the desired frame location [13, 14]. The lunar F-factor calculation is based on irradiance, which is unlike the SD F-factor calculation; the averaged lunar radiance needs to be converted to irradiance units by applying an effective solid angle correction as shown Equation (3).

$$Lunar\ F\text{-}factor(t) = \frac{I_{GIRO}(t)}{L_{avg}(t)\cdot\frac{\pi\cdot R_{moon}^2}{Dist_{Sat-Moon}^2(t)}\cdot\frac{1+\cos(\varphi)}{2}} \quad (3)$$

In Equation (3), the band dependent lunar irradiances are provided by the Global Space-based Inter-Calibration System (GSICS) Implementation of the RObotic lunar observatory (GIRO version 1.0.0) developed by US Geological Survey (USGS)and the European Organization for the Exploitation of Meteorological Satellites (EUMETSAT). In the denominator, L_{avg} is the averaged radiance and is calculated by Equation (4) over all moon pixels.

$$L_{avg} = \frac{\sum L_{Moon\ Pixels}}{N_{Moon\ Pixels}} \quad (4)$$

In Equation (3), R_{moon} is moon radius, $Dist_{sat\text{-}moon}$ is distance between satellite and moon and φ is phase angle of the moon. The denominator of Equation (3) represents the effective solid angle of the moon with phase angle modulation. Once the SD and lunar F-factors are calculated, the lunar F-factors are normalized to the SD F-factors to compare long-term trends.

III. Surface Roughness Rayleigh Scattering (SRRS) Simulation and RSR Effects on SD Degradation

A. *SRRS Based SD Degradation Model Development*

Before running a simulation, the surface roughness parameters were evaluated from the SRRS model by fitting to the current NOAA-20 VIIRS H-factors derived from Equation (1). Figure 3 shows NOAA-20 H-factors from each SDSM detector. Initially, the raw H-factors are fitted to the SRRS model with two variables of surface roughness factor called *R(t)* and the order of the wavelength *n* as shown in Equation (5).

$$\frac{R(t)}{\lambda^n} = 1 - H(t,\lambda) \quad (5)$$

The best curve fit parameters of the wavelength exponent *n* and *R* are derived in each SD degradation estimation point from the SDSM collections. In each SDSM collection, the SRRS model is fitted. Figure 4 shows examples of the H-factors at the SDSM detector wavelengths and the SRRS model fits on 200, 400 and 600 days. Initially, the best fitting wavelength exponent values showed a very noisy pattern but later on they were stabilized around 4 after 300 days in Figure 5. Figure 6 shows the surface roughness R gradually increased with time at an approximate rate of 0.018 μm^2 per year. Equation 6 is the final SRRS model that was used for the degradation simulation.

$$SRRS(t,\lambda) = 1 - \frac{0.018\ t[\mu m^2/\mathrm{year}]}{\lambda^{4.0}} \quad (6)$$

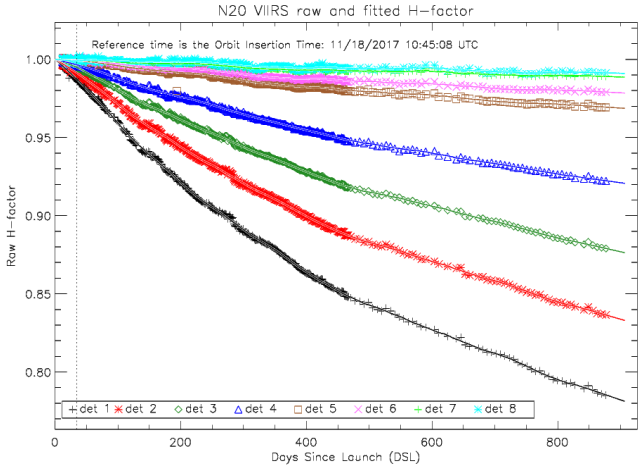

Figure 3. NOAA-20 VIIRS raw and fitted H-factors.

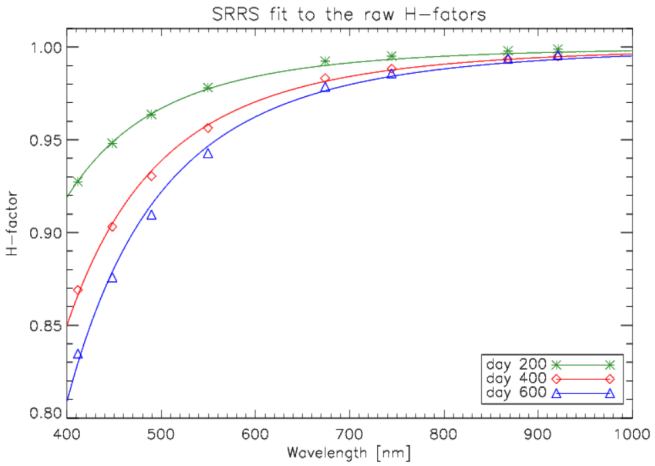

Figure 4. The SRRS model fit to the raw H-factors on selected days.

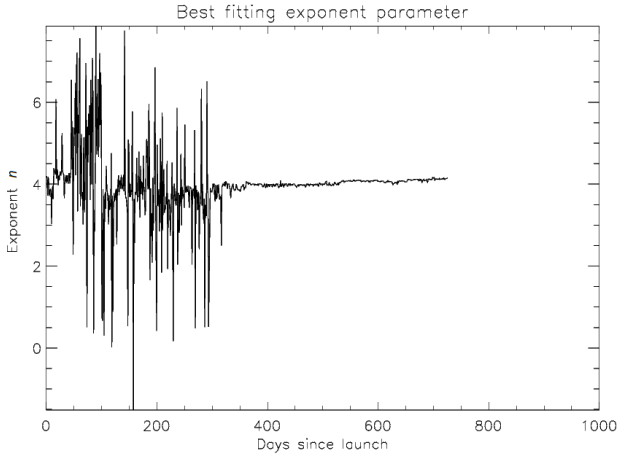

Figure 5. NOAA-20 VIIRS SD SRRS model exponent fit.

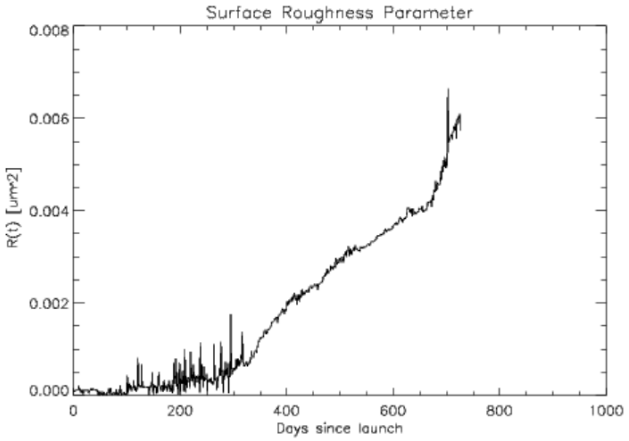

Figure 6. NOAA-20 VIIRS SD Surface roughness factor R(t).

B. Current H-factor and SDSM RSR Dependent SD Degradation Estimation

The H-factors shown in Figure 7 are derived from the SDSM detectors at fixed center wavelengths that were determined from prelaunch testing. The fixed center wavelengths were measured from the detector RSR at the center wavelength of the Full-Width at Half-Maximum (FWHM). When considering the fast degradation of the SD surface short wavelengths according to the SRRS model, the H-factors can be easily changed by the shape of the SDSM detector RSRs.

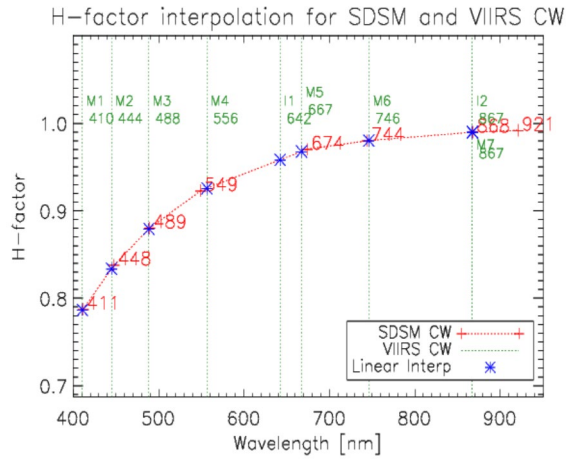

Figure 7. Linear interpolation between SDSM detector center wavelengths and VIIRS band center wavelengths over the SD degradation on March 20, 2020.

There are center wavelength differences between the SDSM and VIIRS detectors. A linear interpolation is applied to get SD degradation (H-factor) at VIIRS center wavelengths from the SDSM center wavelengths shown in Figure 7 as vertical dotted lines. There are spectrally similar bands (I2 and M7) that the Center Wavelength (CW) lines are overlapped in Figure 7. The SDSM and VIIRS center wavelengths are designed to be identical.

To estimate exact amount of SD degradation differences, a wavelength dependent SD degradation is measured each day from the NOAA-20 VIIRS specified SRRS model using Equation 6. Once the true wavelength dependent SD degradation is found, two different H-factor derivation algorithms were tested. The first approach uses the current center wavelength-based algorithm at the CW of the SDSM detector RSR FWHM (CW_{FWHM}) as described in Equation 7.

$$\mathrm{H_{CW}}(\mathrm{Det},\mathrm{t}) = SRRS(CW_{FWHM}, t) \tag{7}$$

The second approach is shown in Equation 8 and it is based on a weighted sum of the SDSM RSR to the SRRS model over the RSR wavelengths.

$$\mathrm{H_{RSR}}(\mathrm{Det},\mathrm{t}) = \frac{\int RSR(\lambda)SRRS(\lambda,t)d\lambda}{\int RSR(\lambda)d\lambda} \tag{8}$$

For NOAA-20 VIIRS SDSM detectors, there were some minor spectral leaks, which may affect the estimated degradation over the wavelength range. Based on these two H-factors, SD F-factors were reprocessed and are compared to the lunar F-factors to check the long-term consistency between the F-factors.

IV. Results

A. SRRS Simulation on the H-factor Algorithms Evaluations

As mentioned in Section III, the true time-dependent SD degradation (H-factor) is simulated by using the SRRS model with an exponent equal to four and a roughness factor of 0.018μm^2 per year as shown in Equation 6. Daily H-factors were calculated using the SRRS over the SDSM detector RSR measurement range. Figure 8 shows the yearly H-factors with the black solid lines that are assumed the true simulated H-factors. Once the reference H-factor is ready, the two H-factor estimation algorithms, H_{CW} and H_{RSR}, are evaluated at the SDSM detector CWs according to Equation 7 and by using the weighted sum approach as described in Equation 8, respectively. For the H_{CW} algorithm, the NOAA-20 SDSM detector CWs are shown as dotted lines in Figure 8. Please note that the SDSM RSRs are established with Gaussian functions because the actual SDSM RSR data are not publicly available. For the SRRS simulation, the measured SDSM detector RSRs with spectral leaks are used to get the H_{CW} and H_{RSR} evaluations. Figure 9 shows the simulated H_{CW} and H_{RSR} results over 10 years. There are growing time-dependent differences especially with the short wavelength detectors from 1 to 4. These

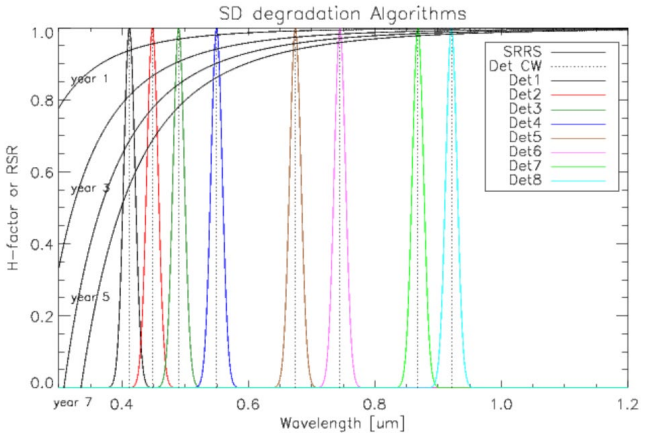

Figure 8. The SRRS simulation of the H-factor estimation algorithms for the CW method and the RSR weighted sum approach. Note that the SDSM detector RSRs are not real response but made up for visualization purpose using Gaussian functions

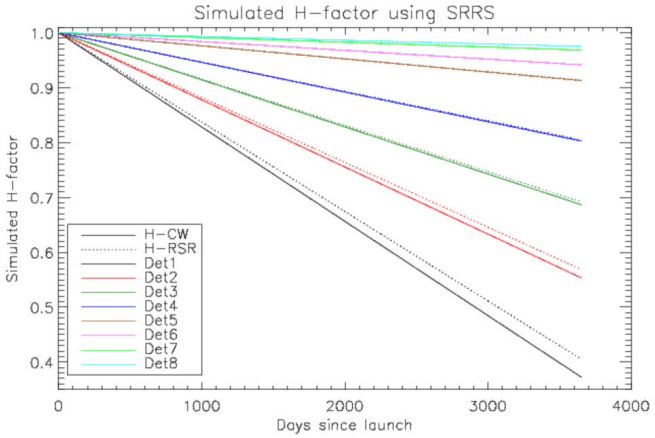

Figure 9. Time-dependent SRRS simulation result over 10 years of operation. The solid lines represent H_{CW} and dotted lines represent H_{RSR} simulation result.

increasing differences are understandable when considering the small Out-Of-Band (OOB) responses in the real SDSM RSR profiles. Especially for SDSM detector 1, there are some OOB spectral leaks around 500nm, 630nm and 800nm. These leaks increased the final H_{RSR} estimation when compared to H_{CW}. Detector 2, 3 and 4 have OOB spectral leaks around 600nm and Detector 2 showed some RSR response around 800nm. The differences between H_{CW} and H_{RSR} are minimal (less than 0.2 percent) for SDSM detectors 5 to 8.

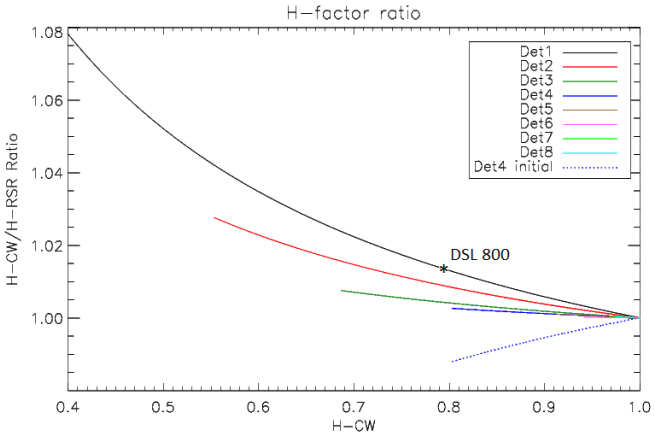

Figure 10. The ratio between H_{CW} and H_{RSR} over H_{CW}.

The H-factor ratios between the two methods as functions of HCW are shown in Figure 10. These results indicate that the current H-factor shown in Figure 3 overestimated the SD degradation up to 1.5 percent in SDSM detector 1 around DSL 800. Since the SD degradation rate exponentially drops toward the short wavelength side, the OOB spectral leaks in the longer wavelength side raise the H_{RSR} over the RSR wavelength. For SDSM detector 4, initial simulation results are shown as the blue dotted line in Figure 10. The direction of the ratio was different from other detectors. When the SDSM detector 4 RSR shape was tested, there were small constant spectral leaks in the short wavelength side of the main lobe below 470nm. There were multiple measurements of the SDSM detector RSR and one measurement (called the far filed) did not show the short wavelength spectral leaks below 470nm. The spectral leaks could be caused by the measurement errors in the prelaunch test. After removing these spectral leaks, the direction of H-factor ratio back to normal as shown by the blue solid line in Figure 8. The RSR OOB effects are most effective in SDSM detectors 1 to 4, whereas changes are less than 0.2 percent level over 10 years of simulation in SDSM detectors 5 to 8.

B. H-factor to H_{RSR} Conversion Using Simulated Ratio

Using the simulated H_{ratio} as shown in Figure 10, the RSR applied H-factor is derived in each SDSM detector using Equation 9. Please note that the H_{ratio} is a function of H_{CW}.

$$H_{RSR\_new}(t) = H\text{-}factor(t) H_{Ratio}[H_{CW}(t)] \qquad (9)$$

As expected from the simulation result, the corrected H_{RSR_new} show smaller degradation than the original ones as shown in Figure 11 .

C. SD and lunar F-factor comparison results

The VIIRS radiometric calibration in RSBs is primarily dependent on SD F-factors that are calculated from the daily SD observations. As shown in Equation 2, SD F-factors are linearly related to the H-factor changes, which also directly affect Earth View radiance. The normal SD and lunar F-factors are shown as lines in Figure 12 without applying H_{RSR}. The lunar F-factors (symbols) are normalized to the SD F-factors at the second collection of the lunar collection on January 27, 2018. There are gaps in the lunar F-factors from June to October. Details of the

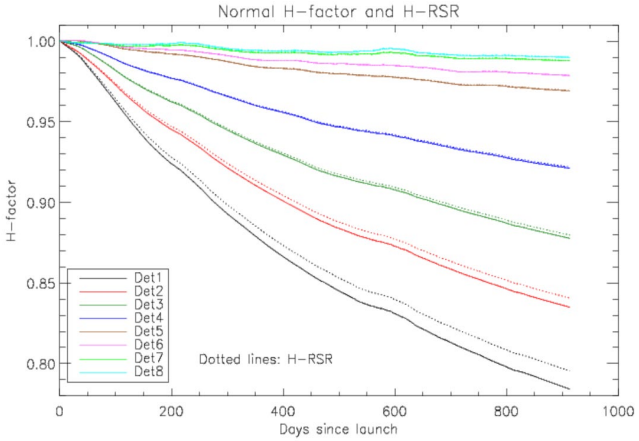

Figure 11. The derived H_{RSR_new} from the normal H_{CW} using the simulated ratio. The solid lines represent previous (normal) H-factor, whereas the dashed lines represent H_{RSR}.

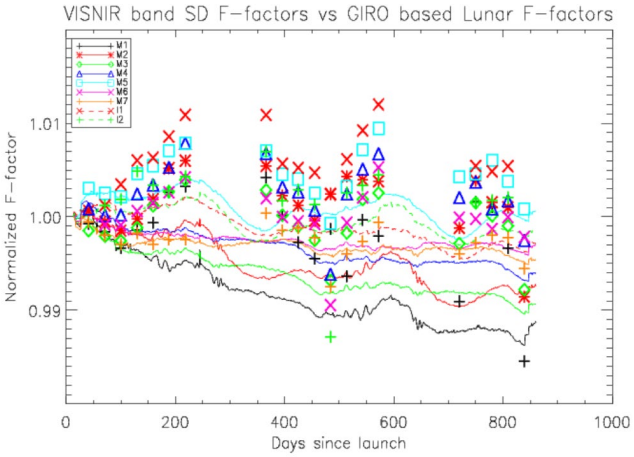

Figure 12. Lunar F-factors (symbols) and SD F-factors (lines) without H-RSR_new correction.

NOAA-20 lunar calibration results were reported in previous work [14]. Even though there are different patterns in the oscillations, the SD and lunar F-factors show similar long-term trends mostly within ±1 percent. Additionally, there are growing differences between the lunar and SD F-factors in the short wavelength bands of M1 to M4. Especially, the black lines (band M1) shows the largest deviation--slightly more than 1 percent.

With the SDSM detector RSRs and VIIRS RSRs, the new H_{RSR} is applied to the SD F-factor. In Figure 13, the newly corrected SD F-factors are entirely reprocessed with the normalized lunar F-factors. First of all, the SD and lunar F-factor deviations in the short wavelength are mostly flattened especially in bands M1 to M4. After the correction, the SD F-factors are stabilized in the short wavelength bands mostly within ±0.5 percent and follow the long-term lunar F-factors.

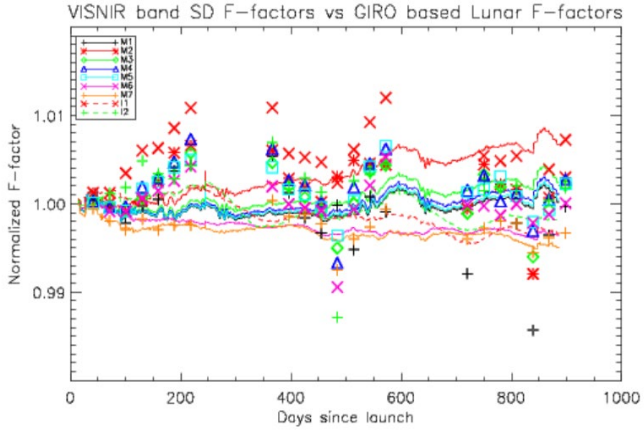

Figure 13. Lunar F-factors (symbols) and SD F-factors (lines) with H-RSR_new correction.

V. Conclusions

Using SDSM detector RSRs and the SRRS model, an improved SD degradation algorithm is developed and applied to NOAA-20 RSB radiometric calibration. Because of the OOB responses, the SDSM detector RSRs increased the new SD degradation (H-RSR) up to 1.5 percent in the shortest wavelength detector of the SDSM.

The SD degradation simulation with the SDSM RSR and CW-based approaches show the level accuracy of the prelaunch SDSM RSR and OOB response measurements. The exponentially fast degradations in the short wavelengths cause the non-linear behavior of the degradation differences. These simulation results are applied to the on-orbit radiometric calibration called SD F-factors and the long-term SD F-factor trends are validated from the independent lunar calibration. With the RSR-based SD degradation, the long-term trend differences between lunar and SD F-factors are significantly reduced in the short wavelength bands M1 to M4. In band M1, the H-factor correction improved the differences from 1.5 percent to 0.2 percent. The corrected SD F-factors and lunar F-factors showed very stable RSB responses over two years of RSB radiometric calibration.

With the known large OOB responses in the JPSS-2 VIIRS SDSM RSRs, this algorithm can be applied to estimate actual SD degradation over the operational wavelength range reducing the possible differences between SD and lunar radiometric calibrations.

VI. Disclaimer

The scientific results and conclusions, as well as any views or opinions expressed herein, are those of the author(s) and do not necessarily reflect those of NOAA or the Department of Commerce.

VII. References

[1] X. Xiaoxiong, C. Kwo-Fu, W. Aisheng, W. L. Barnes, B. Guenther, and V. V. Salomonson, "Multiyear On-Orbit Calibration and Performance of Terra MODIS Thermal Emissive Bands," *IEEE Transactions on Geoscience and Remote Sensing,* vol. 46, no. 6, pp. 1790-1803, 2008.

[2] X. Xiaoxiong, S. Junqiang, X. Xiaobo, W. L. Barnes, and V. V. Salomonson, "On-Orbit Calibration and Performance of Aqua MODIS Reflective Solar Bands," *IEEE Transactions on Geoscience and Remote Sensing,* vol. 48, no. 1, pp. 535-546, 2010.

[3] X. Xiong, A. Angal, T. Choi, X. Gu, J. Sun, and E. Johnson, "On-orbit performance of MODIS solar diffuser stability monitor," presented at the Earth Observing Systems XVII, 2012.

[4] S. Lee and G. Meister, "MODIS solar diffuser degradation determination and its spectral dependency," presented at the Earth Observing Systems XXIII, 2018.

[5] B. Markham *et al.*, "Landsat-8 Operational Land Imager Radiometric Calibration and Stability," *Remote Sensing,* vol. 6, no. 12, pp. 12275-12308, 2014.

[6] T. Choi, X. Shao, and C. Cao, "On-orbit radiometric calibration of Suomi NPP VIIRS reflective solar bands using the Moon and solar diffuser," *Appl Opt,* vol. 57, no. 32, pp. 9533-9542, Nov 10 2018.

[7] C. Bruegge, A. Stiegman, R. Rainen, and A. Springsteen, "Use of Spectralon as a diffuse reflectance standard for in-flight calibration of earth-orbiting sensors," vol. 32 %J Optical Engineering, no. 4, 1993.

[8] F. Yu and X. Wu, "Radiometric Inter-Calibration between Himawari-8 AHI and S-NPP VIIRS for the Solar Reflective Bands," *Remote Sensing,* vol. 8, no. 3, 2016.

[9] X. Shao *et al.*, "Validation of GOES-16 ABI reflective solar band calibration through reanalysis and comparison with field campaign data," presented at the Earth Observing Systems XXIII, 2018.

[10] H. Erives, X. Xiong, J. Sun, J. A. Esposito, S. Xiong, and W. L. Barnes, "Terra MODIS RSB on-orbit calibration and performance: four years of data," presented at the Sensors, Systems, and Next-Generation Satellites VIII, 2004.

[11] J. Sun and M. Wang, "VIIRS Reflective Solar Bands Calibration Progress and Its Impact on Ocean Color Products," *Remote Sensing,* vol. 8, no. 3, 2016.

[12] X. Xiong, J. Sun, J. Fulbright, Z. Wang, and J. J. Butler, "Lunar Calibration and Performance for S-NPP VIIRS Reflective Solar Bands," *IEEE Transactions on Geoscience and Remote Sensing,* vol. 54, no. 2, pp. 1052-1061, 2016.

[13] T. Choi, C. Cao, and F. Weng, "RADIOMETRIC STABILITY MONITORING OF THE S-NPP VIIRS OCEAN COLOR BANDS USING THE MOON," presented at the International Symposium on Remote Sensing (ISRS), Jeju, Korea, April 20, 2016.

[14] T. Choi, X. Shao, S. Blonski, W. Wang, S. Uprety, and C. Cao, "NOAA-20 VIIRS initial on-orbit radiometric calibration using scheduled lunar observations," presented at the Earth Observing Systems XXIV, 2019.

[15] F. Weng, T. Choi, C. Cao, and B. Zhang, "Reprocessing of SUOMI NPP VIIRS sensor data records and impacts on environmental applications," in *2017 IEEE International Geoscience and Remote Sensing Symposium (IGARSS)*, 2017, pp. 293-296.

[16] T. Choi, X. Shao, C. Cao, and F. Weng, "Radiometric Stability Monitoring of the Suomi NPP Visible Infrared Imaging Radiometer Suite (VIIRS) Reflective Solar Bands Using the Moon," *Remote Sensing,* vol. 8, no. 1, 2015.

[17] J. Sun, M. Chu, and M. Wang, "Degradation nonuniformity in the solar diffuser bidirectional reflectance distribution function," *Appl Opt,* vol. 55, no. 22, pp. 6001-16, Aug 1 2016.

[18] N. Lei and X. Xiong, "Impacts of the Angular Dependence of the Solar Diffuser BRDF Degradation Factor on the SNPP VIIRS Reflective Solar Band On-Orbit Radiometric Calibration," *IEEE Transactions on Geoscience and Remote Sensing,* vol. 55, no. 3, pp. 1537-1543, 2017.

[19] J. Sun and M. Wang, "Radiometric calibration of the Visible Infrared Imaging Radiometer Suite reflective solar bands with robust characterizations and hybrid calibration coefficients," *Appl Opt,* vol. 54, no. 31, pp. 9331-42, Nov 1 2015.

[20] X. Shao, C. Cao, and T.-C. Liu, "Spectral Dependent Degradation of the Solar Diffuser on Suomi-NPP VIIRS Due to Surface Roughness-Induced Rayleigh Scattering," *Remote Sensing,* vol. 8, no. 3, 2016.

[21] X. Shao, T.-C. Liu, X. Xiong, C. Cao, T. Choi, and A. Angal, "Surface Roughness-Induced Spectral Degradation of Multi-Spaceborne Solar Diffusers Due to Space Radiation Exposure," *IEEE Transactions on Geoscience and Remote Sensing,* pp. 1-14, 2019.

[22] T. J. Hewison *et al.*, "Extending the Global Space-Based Inter-Calibration System (GSICS) to Tie Satellite Radiances to an Absolute Scale," *Remote Sensing,* vol. 12, no. 11, 2020.

[23] G. Chander *et al.*, "Applications of Spectral Band Adjustment Factors (SBAF) for Cross-Calibration," *IEEE Transactions on Geoscience and Remote Sensing,* vol. 51, no. 3, pp. 1267-1281, 2013.

[24] N. Baker and H. Kilcoyne, "Joint Polar Satellite System (JPSS) VIIRS Radiometric Calibration Algorithm Theoretical Basis Document (ATBD)," J. P. S. S. J. G. Project, Ed., ed. NOAA and NASA: NOAA & NASA, 2011.

[25] T. Choi, S. Blonski, X. Shao, and C. Cao, "Improving NOAA 20 VIIRS screen transmittance and solar diffuser BRF estimation from both Yaw maneuver and regular on-orbit data," in *SPIE Remote Sensing*, 2018, vol. 10785, p. 15: SPIE.

[26] T. Choi, S. Blonski, and C. Cao, "Initial on-orbit radiometric calibration of the NOAA-20 VIIRS Reflective Solar Bands," in *SPIE Optical Engineering + Applications*, 2018, vol. 10764, p. 11: SPIE.

[27] T. Choi, C. Cao, S. Blonski, W. Wang, S. Uprety, and X. Shao, "NOAA-20 VIIRS Reflective Solar Band Postlaunch Calibration Updates Two Years In-Orbit," *IEEE Transactions on Geoscience and Remote Sensing,* pp. 1-10, 2020.